Supporting Information

Brain systems for baroreflex suppression during stress in humans

Peter J. Gianaros[1†], Ikechukwu C. Onyewuenyi[2], Lei K. Sheu[1], Israel C. Christie[1], and Hugo D. Critchley[3,4,5]

[1]Department of Psychiatry, University of Pittsburgh, 3811 O'Hara Street, Pittsburgh, PA 15213. [2]Department of Psychology, University of Pittsburgh, 15260, Pittsburgh, PA. [3]Department of Psychiatry, Brighton and Sussex Medical School, University of Sussex Campus, Falmer, Brighton BN1 3AR, UK. [4]Sackler Centre for Consciousness Science, University of Sussex. [5]Sussex Partnership NHS Foundation Trust

Table S1

Brain areas where greater relative BOLD activation identified by the 'Incongruent > Congruent' condition contrast covaried with a greater decrease in baroreflex sensitivity in a whole-brain and exploratory multiple regression analysis with covariate control for age, sex, and resting baroreflex sensitivity.

Side	Region	BA	MNI coordinates (peak)			t-value	voxels
			x	y	z		
L/R	Perigenual anterior cingulate cortex	32	0	44	-4	3.98	237
	Medial prefrontal cortex	10	6	58	-6	4.44	
R	Subgenual anterior cingulate cortex	25	4	18	-10	4.13	61
L/R	Dorsal anterior cingulate cortex	32, 33, 24	4	28	24	4.90	446
R	Posterior mid-cingulate cortex	24,6	10	-4	-44	4.24	85
L/R	Posterior mid-cingulate cortex	24	6	-6	-28	3.80	106
L/R	Posterior cingulate cortex	29, 30	-2	-44	20	4.04	112
L	Posterior insula	13	-44	-24	-6	4.12	1816
R	Postcentral gyrus	43	62	-8	16	4.94	1503
R	Superior temporal gyrus	38	40	2	-18	4.08	59
R	Post-central gyrus,	2	36	-28	38	4.73	988
	Pre-central gyrus	3	26	-28	56	4.46	
		4	48	-14	38	4.50	
L	Posterior insula	13	-38	-36	20	4.51	149
R	Amygdala		20	-2	-22	4.42	58
L	Hippocampus	28,35	-26	-24	-14	4.32	131
R	Fusiform gyrus, Parahippocampal gyrus	37	42	-38	-8	4.16	205
L	Thalamus		-8	-32	10	4.23	156
R	Thalamus		8	-32	8	3.72	146
R	Thalamus		8	-8	16	3.56	111
R	Caudate nucleus, Putamen		18	22	0	3.76	92
R	Inferior parietal lobule	40	56	28	40	4.03	62
L	Cuneus	18	-22	-68	20	3.96	88
L	Inferior frontal gyrus	45	-50	28	-2	3.77	305
R	Middle frontal gyrus	6	38	14	48	3.70	97
L	Middle temporal gyrus	19,39	-36	-56	2	3.68	64

Note. Next to each left (L) and right (R) region and approximate Brodmann area (BA) are the MNI coordinates (for the peak voxel in each cluster), where x = right (+) to left (-); y = anterior (+) to posterior (-); z = superior (+) to inferior (-).T-values for voxels of peak activation and their corresponding cluster extents were derived from a mixed-effects analysis employing a height threshold of $P<0.001$ and extent cluster threshold of $k = 50$ voxels (see Figure S3).

Table S2

(a) Brain areas exhibiting relative BOLD activation identified by the 'Incongruent > Congruent' condition contrast in a random-effects model.

Side	Region	BA	MNI coordinates (peak)			t-value	voxels
			x	y	z		
L/R	Dorsal mid-anterior cingulate cortex	24	-8	14	44	10.07	10627
	Superior frontal gyrus	6	6	12	48	10.60	
	Pre-central gyrus	6	-44	4	28	10.32	
	Anterior insula	13	-32	20	4	7.49	
	Anterior insula	13	34	24	0	5.61	
L/R	Precuneus	7	-8	-74	50	9.76	13805
	Angular gyrus	39	-32	-54	46	9.50	
	Cerebellum		-34	-70	-24	9.68	
L/R	Thalamus		-12	-16	6	7.15	1023
			8	-14	8	6.17	
(b) Brain areas exhibiting BOLD relative deactivation identified by 'Congruent > Incongruent' condition contrast in a random-effects model							
L/R	Posterior cingulate	31, 23	-6	-40	34	10.2	5862
	Amygdala, hippocampus	28	-22	-20	-24	8.56	
L/R	Perigenual/subgenual anterior cingulate cortex	32	-2	46	-18	9.90	4106
	Orbitomedial prefrontal cortex	24	-4	30	-12	8.33	
		25	0	18	-10	7.43	
L	Posterior insula	13	-38	-18	18	8.85	1227
	Middle temporal gyrus	21	-46	4	-34	5.20	
R	Posterior insula	13	38	-18	-16	7.5	1607
L	Superior frontal gyrus	8	-24	32	48	8.25	1057
L	Angular gyrus, middle temporal gyrus	39	-46	-72	36	10.67	735
R	Parahippocampal gyrus	34	20	-14	-24	6	59
R	Superior and middle frontal gyrus	8	20	40	50	6.20	487
		6	26	32	52	5.43	
		4	14	-34	68	4.49	307
L/R	Paracentral lobule	5	-4	32	60	3.87	
		6	8	-22	68	4.11	

Note. Next to each left (L) and right (R) region and approximate Brodmann area (BA) are the MNI coordinates (for the peak voxel in each cluster), where x = right (+) to left (-); y = anterior (+) to posterior (-); z = superior (+) to inferior (-). T-values for voxels of peak activation / relative deactivation and their corresponding cluster extents were derived from a random-effects analysis employing a false detection rate of 0.05, based on Monte Carlo simulations (see Materials and Methods and Figure S4). For each contrast, these height and extent thresholds corresponded to $P<0.001$ and $k = 206$ voxels.

Table S3

(a) Areas showing significantly greater functional connectivity with a perigenual anterior cingulate cortex seed during the performance of the incongruent condition of the MSIT (see Figure S5)

Side	Region	BA	MNI Coordinates			t-value	Voxels
			x	y	z		
L	Superior/middle frontal gyrus	10	16	40	-14	5.40	5741
R	Superior/middle frontal gyrus	10	-18	56	-8	4.60	
R	Inferior/middle frontal gyrus	47	46	38	-6	4.29	
L	Inferior/middle frontal gyrus	46, 47	-50	28	24	3.86	
			-18	36	-14	5.26	
L	Subgenual/perigenual anterior cingulate		-8	32	-2	4.22	
R	Subgenual/perigenual anterior cingulate		8	34	-6	4.05	
L/R	Caudate head		-16	26	-12	4.64	
R	Midbrain		12	-16	-6	4.07	
L	Midbrain		-8	-16	-8	3.57	
R	Thalamus		6	-6	14	3.73	
L	Globus pallidus		-14	-4	-2	4.51	
L	Caudate body		-6	14	4	4.31	
R	Caudate body		8	14	6	4.09	
L	Pre-central gyrus	4	-40	-16	36	3.20	281
L	Inferior parietal lobule	40	-36	-34	30	3.14	
R	Inferior temporal gyrus, Fusiform gyrus	37	56	-58	-4	4.18	152
R	Pre-central gyrus	6	44	32	18	4.17	1451
R	Medial frontal gyrus	6	16	8	54	4.15	127
R	Inferior parietal lobule	40	-38	-50	40	3.92	711
L	Posterior cingulate gyrus	31	-16	-28	36	3.53	
L	Caudate Tail		38	-36	8	3.78	70
R	Posterior cingulate gyrus	31	18	-26	46	3.60	54
R	Precuneus	7	10	-50	54	3.36	59
(b) Areas showing significantly greater functional connectivity with an amygdala seed during the performance of the incongruent condition of the MSIT (see Figure S6)							
R	Inferior/middle temporal gyrus	37	48	-44	-6	4.71	2611
L	Anterior insula	13	-32	16	14	3.94	
L	Putamen		-20	8	12	4.1	
R	Parahippocampal gyrus	35,28, 34	32	-30	-24	4.36	
L/R	Thalamus		2	-4	2	3.97	

R	Thalamus		18	-16	6	3.72	
L/R	Cerebellum		-16	-50	-10	4.11	766
R	Hippocampus		32	-38	-4	3.31	
L	Medial globus pallidus		-10	0	-4	3.95	
R	Lateral globus pallidus		26	-18	-6	3.42	
L/R	Midbrain		4	-30	-18	3.22	
L	Pons		-12	-16	-26	3.74	
L	Fusiform gyrus	20	-46	-8	-26	4.02	651
L	Sub-Gyral	21	-46	-18	-16	4.02	
L	Caudate Tail		-34	-16	-12	3.92	
L	Thalamus		-20	-8	14	3.92	126
R	Thalamus		4	-24	16	3.7	95
L	Posterior insula	13	-34	-22	22	3.84	178
L	Pre-central gyrus	6	-42	-6	26	3.17	
R	Caudate body		-24	-20	26	3.02	
R	Occipital Lobe	19	32	-70	-2	3.73	50
R	Middle temporal gyrus	22	46	-20	-10	3.71	67
L	Caudate body		-8	-6	20	3.11	
L	Precuneus	31	-18	-40	34	3.56	181
L	Posterior cingulate gyrus	31	-22	-50	30	3.52	
L	Caudate Tail		-20	-30	26	3.06	
R	Putamen		26	14	6	3.03	55
R	Hypothalamus		10	-2	-12	3.09	50
R	Amygdala		34	-2	-28	3.52	55
R	Posterior cingulate gyrus	31	24	-34	28	3.45	63
L	Superior temporal gyrus	39, 22	-46	-50	24	3.38	127
L	Middle temporal gyrus	19	-34	-60	14	3.29	
(c) Areas showing significantly greater functional connectivity with a left anterior insula seed during the performance of the incongruent condition of the MSIT (see Figure S7)							
R	Middle temporal gyrus/Fusiform gyrus	19, 20, 21	48	-4	-28	5.26	9120
L	Middle temporal gyrus/Fusiform gyrus	21, 37	-50	-2	-24	3.8	
L	Insula/Inferior frontal gyrus	45, 47	-34	18	-16	4.5	
R	Insula/Inferior frontal gyrus	47	38	18	-16	3.41	
R	Parahippocampal gyrus	28, 34	30	-20	-24	4.3	
L	Parahippocampal gyrus	28, 34	-22	-24	-26	3.81	

L/R	Cerebellum		46	-58	-24	4.43	
R	Pons		6	-22	-32	4.44	
L	Midbrain (PAG)		-14	-28	-6	4.15	
L	Postcentral gyrus	2,3	-32	-22	46	4.43	422
R	Postcentral gyrus	2	46	-22	26	3.33	53
R	Insula/Superior temporal gyrus	13, 22	42	-42	22	4.3	176
L	Cingulate gyrus/Precuneus	31	-10	-50	38	3.88	591
R	Angular gyrus	39	36	-64	22	4.08	165
L	Middle occipital gyrus	18, 19	-24	-88	0	3.73	81
L	Medial globus pallidus		-12	0	-2	3.67	212
L	Caudate Body		-12	4	8	3.52	
L	Thalamus		-16	-4	14	3.3	
L	Thalamus		-16	-4	14	3.3	
(d) Areas showing significantly greater functional connectivity with a dorsal anterior cingulate seed during the performance of the incongruent condition of the MSIT (see Figure S8)							
L	Middle frontal gyrus (DLPFC)	46	-48	32	22	4.78	762
R	Inferior frontal gyrus(DLPFC)	46	36	12	22	4.25	159
R	Superior frontal gyrus	9	16	48	28	4.24	334
R	Middle frontal gyrus (DLPFC)	46	44	28	20	4.17	278
L	Medial frontal gyrus	9	-8	42	30	3.92	72
R	Orbitofrontal cortex	11	40	38	-12	3.65	65
L	Rostral anterior cingulate cortex	32	-8	30	40	3.57	87
R	Superior frontal gyrus	8	38	14	54	3.46	169
R	Inferior parietal cortex	40	36	-56	48	3.38	103
L	Posterior insula	13	-32	-18	26	3.18	84

Note. Next to each left (L) and right (R) region and approximate Brodmann area (BA) are the MNI coordinates of the peak voxel in the cluster, where x = right (+) to left (-); y = anterior (+) to posterior (-); z = superior (+) to inferior (-). T-values for voxels of peak connectivity and their corresponding cluster extents were derived from a random-effects analysis employing a family-wise error rate corrected threshold of $P<0.005$ with an extent threshold of $k = 50$ voxels.

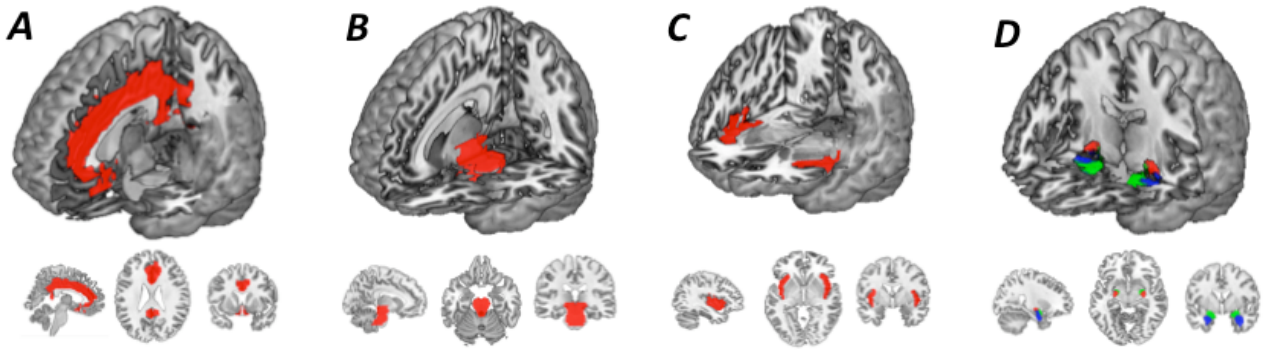

Figure S1. Region-of-interest (ROI) analyses were executed for tests of the covariation between the change in baroreflex sensitivity from baseline to the multi-source interference stressor task and individual differences in the activation and functional connectivity of the cingulate, midbrain/pons, insula, and amygdala. ***A-D***, Illustrations of anatomical masks used for ROI analyses: ***A:*** cingulate, ***B:*** midbrain/pons, ***C:*** insula, ***D***: combined subregions of the amygdala (red: corticomedial [CM]; blue: superficial [SF]; green: basolateral [BL]). ROIs for the cingulate, midbrain/pons, and insula were created using the Talairach Daemon database (Lancaster et al., 1997), as implemented in the WFU Pick-Atlas Toolbox (Maldjian et al., 2003). The amygdala ROI was created using the SPM Anatomy toolbox, combing the SF, CM and BL subregions (Eickhoff et al., 2005). The dimensions for the cingulate ROI had center of mass of x = 1, y = 1, and z = 28. It extended along the x- y- and z- directions from a minimum (min) x coordinate of -16mm to a maximum (max) x-coordinate of 18mm; a min y of -58mm to a max y of 54mm; a min z of -20mm to a max z of 54mm. It had a volume of 62808 mm^3. The combined midbrain and pons ROI had center of mass of 0, -25, -22, and it extended from a min x of -22mm to a max x of 24mm, a min y of -44mm to a max y of -4 mm, and a min z of -42mm to a max z of 0mm. Its volume was 23160mm^3. The insula and amygdala ROIs were bilateral. The left insula ROI was centered at -35, 5, 2, and it extended from a min x of -48mm to a max x of -24mm, a min y of -32mm to a max y of 32mm, and a min z of -20mm to a max z of 22mm. The right insula had center of mass at 39, 5,1, and it extended from a min x of 26mm to a max x of 50mm, a min y of -30mm to a max y of 32mm, and a min z of -20mm to a max z of 22mm. The total volume of the insula ROI was 28664mm^3. The left amygdala ROI had a center of mass at -23,-6, -16. It extended from a min x of -37mm to max x of -18mm, a min y of -15mm to a max y of 3mm, and a min z of -36mm to a max z of -9mm. The right amygdala had center of mass at 26,-5,-16. It extended from min x of 21mm to a max x of 41mm, a min y of -15mm to a max y of 4mm, and a min z of -39mm to a max z of -10mm. The total volume of the amygdala ROI was 6832mm^3. All masks are available on request.

To determine the covariation between (*i*) the change in BRS from baseline to task performance, (*ii*) MSIT-related activation and relative deactivation, as well as (*iii*) PPI functional connectivity at the group level, individual contrast maps (Incongruent vs. Congruent) and connectivity maps generated from seed regions (pACC, amygdala, and anterior insula) were submitted to general linear models in SPM8. For all analyses, we maintained a corrected false-discovery threshold of 0.05 within the volumes of all ROIs by employing voxel-wise and combined cluster extent thresholds determined by the spatial smoothness (in FWHM) and 2000 Monte Carlo simulations implemented in AlphaSim (Ward, 2000) Thresholds needed to account for multiple testing within the ROI volumes for each analysis are below.

Analysis	ROI mask	*P*-value	Extent threshold
Covariation of fMRI BOLD signal change with ΔBRS	Cingulate	0.001	50
	Insula		26
	Amygdala		4
	Midbrain/Pons		19
Connectivity with perigenual anterior cingulate cortex seed (MNI x y z: 0 44 -4)	Insula	0.001	47

Brain systems for baroreflex suppression

Connectivity with right amygdala seed (MNI x y z: -42 18 20)	Insula	0.001	6
Connectivity with left anterior insula seed (MNI x y z: -30 14 14)	Midbrain/Pons	0.001	19

References

Eickhoff S, Stephan KE, Mohlberg H, Grefkes C, Fink GR, Amunts K, Zilles K (2005): A new SPM toolbox for combining probabilistic cytoarchitectonic maps and functional imaging data. NeuroImage 25: 1325-1335.

Lancaster JL, SummerIn JL, Rainey L, Freitas CS, Fox PT (1997): The Talairach Daemon, a database server for Talairach Atlas Labels. NeuroImage 5:S633.

Maldjian JA, Laurienti PJ, Kraft RA, Burdette JH (2003): An automated method for neuroanatomic and cytoarchitectonic atlas-based interrogation of fMRI data sets. NeuroImage 19: 1233-1239.

Ward BD (2000): Simultaneous inference for fMRI data: AFNI 3d Deconvolve documentation. Medical College of Wisconsin.: http://afni.nimh.nih.gov/pub/dist/doc/program_help/3dDeconvolve.html

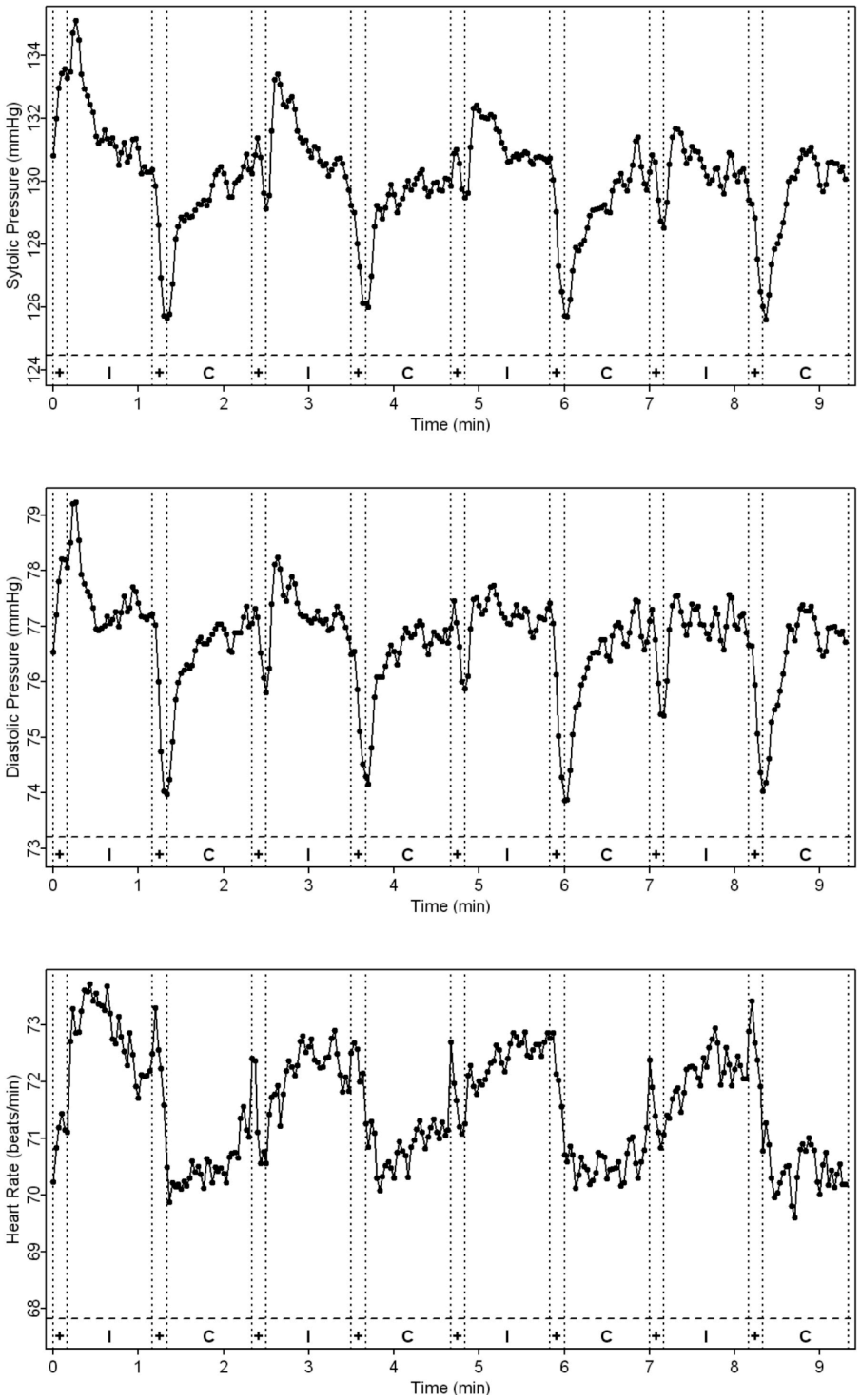

Figure S2. Average time-series for systolic and diastolic blood pressures, and heart rate across the multi-source interference task stressor epochs. Time series were re-sampled at 10Hz, starting at task onset in order to align to a commonly referenced time line across participants. Each time point represents the mean of a 2 sec, non-overlapping window. The dotted vertical lines delineate the fixation (+), congruent (C), and incongruent (I) task epochs. The dashed horizontal lines in each panel represent the mean from the last 5 min of the preceding baseline period for each variable. Random-effects models of epoch means showed that for each of the three variables: 1) levels during the fixation, congruent, and incongruent task epochs were significantly increased relative to baseline ($ts \geq 8.18$; $Ps \leq 0.0001$); and 2) levels during the incongruent epochs were significantly greater than those of the congruent epochs ($ts \geq 2.5876$; $Ps \leq 0.01$).

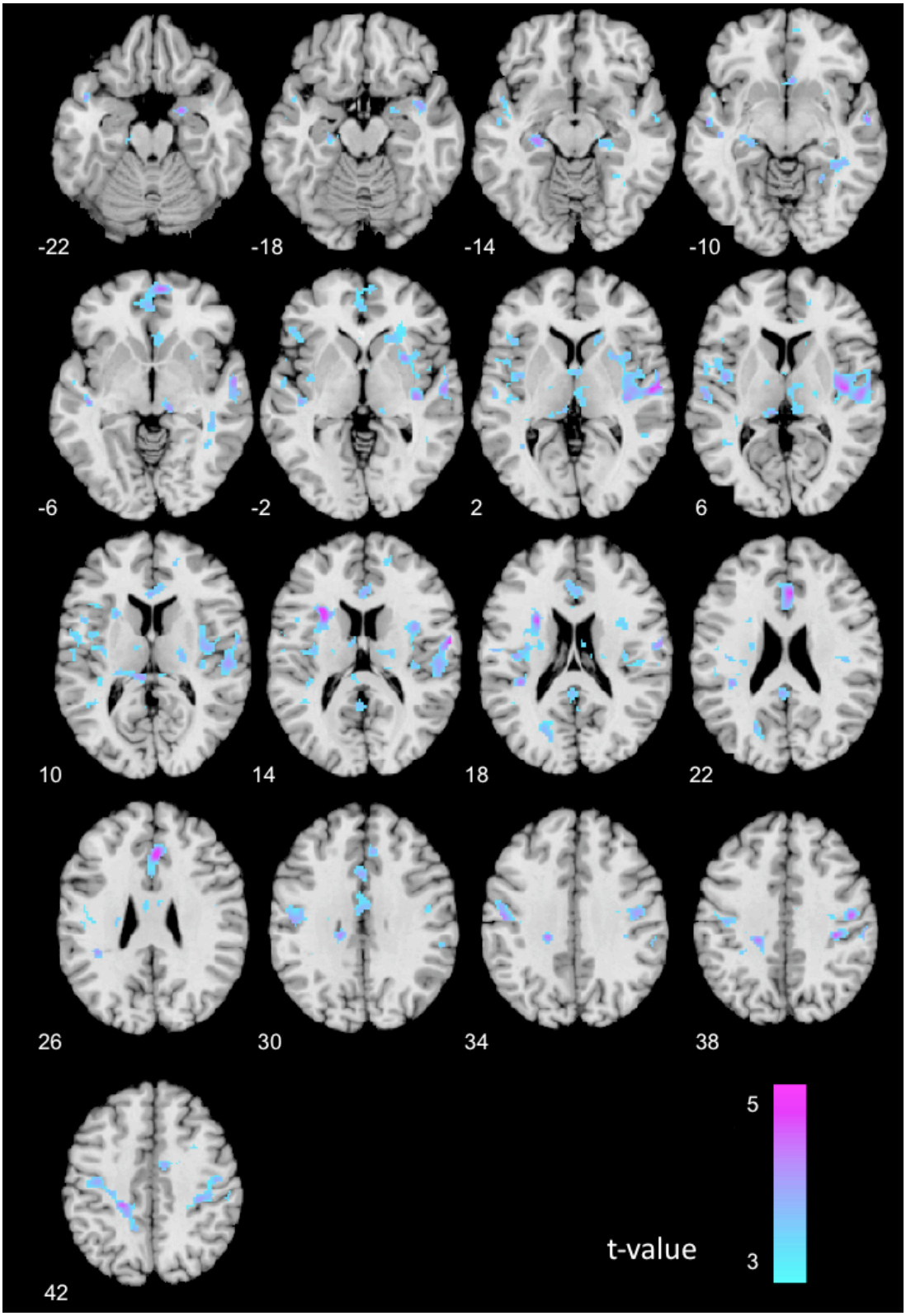

Figure S3. Whole-brain parametric map profiling areas where a greater stressor-evoked reduction in baroreflex sensitivity correlated with greater BOLD activation, as determined by the 'Incongruent > Congruent' contrast in multiple regression analyses. The map is thresholded at an uncorrected $P<0.001$ and $k = 50$. Table S2 provides Brodmann areas, MNI coordinates, and *t*-values for voxels of peak activation (global maxima) profiled in this map. Values in the lower left corner of each slice correspond to *z* coordinates in MNI space.

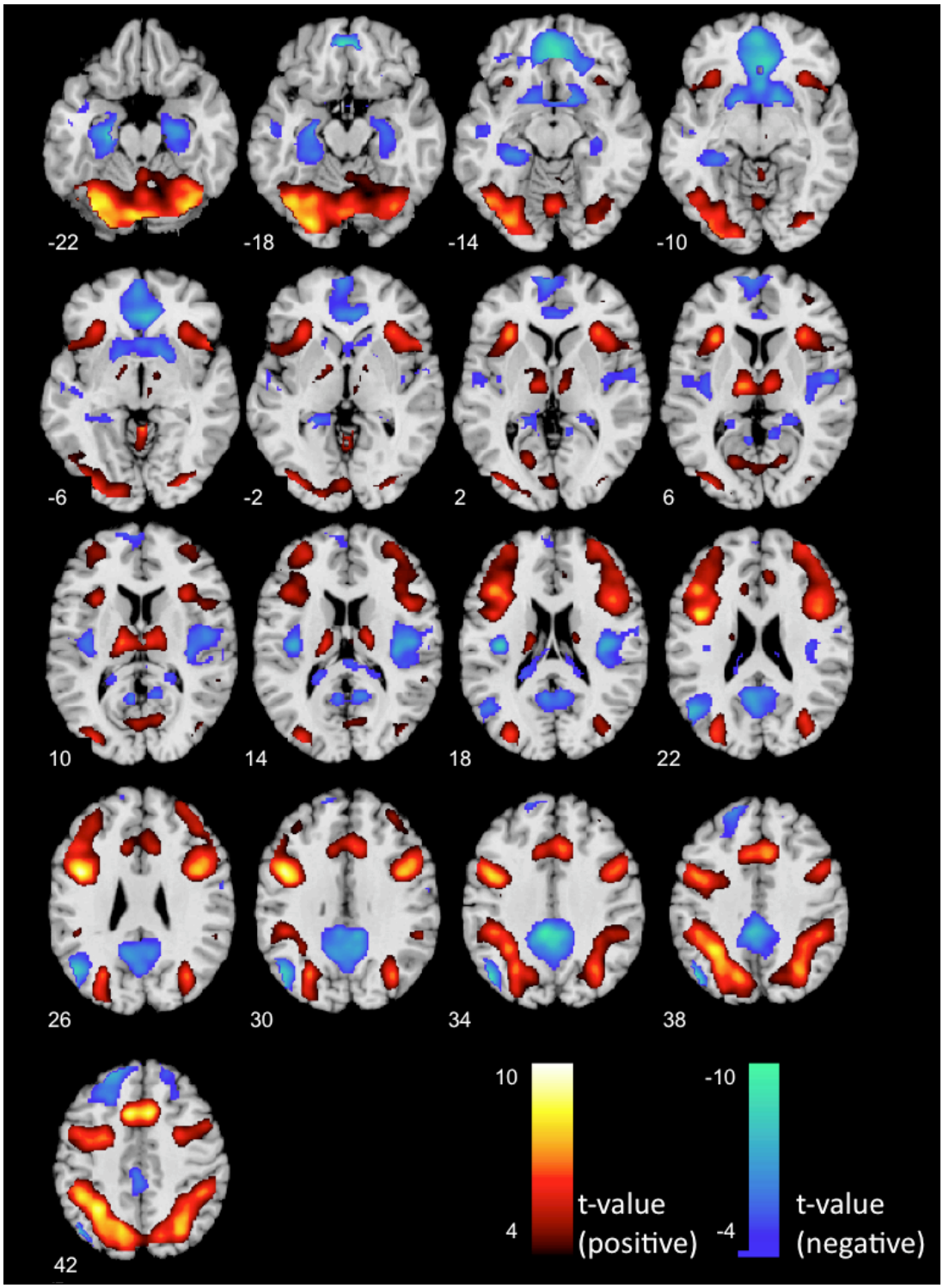

Figure S4. Parametric maps profiling areas of relative BOLD activation (red-yellow) and deactivation (blue-green) determined by the 'Incongruent > Congruent' and the 'Congruent > Incongruent' contrasts in whole-brain random-effects analyses, respectively. Maps are displayed at a corrected voxel-wise threshold of $P<0.05$, determined by Monte Carlo simulations (see Materials and Methods). This threshold corresponded to a voxel-wise $P<0.001$ and combined cluster extent threshold of $k > 206$. Table S3 provides Brodmann areas, MNI coordinates, and *t*-values for voxels of peak activation and deactivation (global maxima) profiled in these maps. Values in the lower left corner of each slice correspond to *z* coordinates in MNI space.

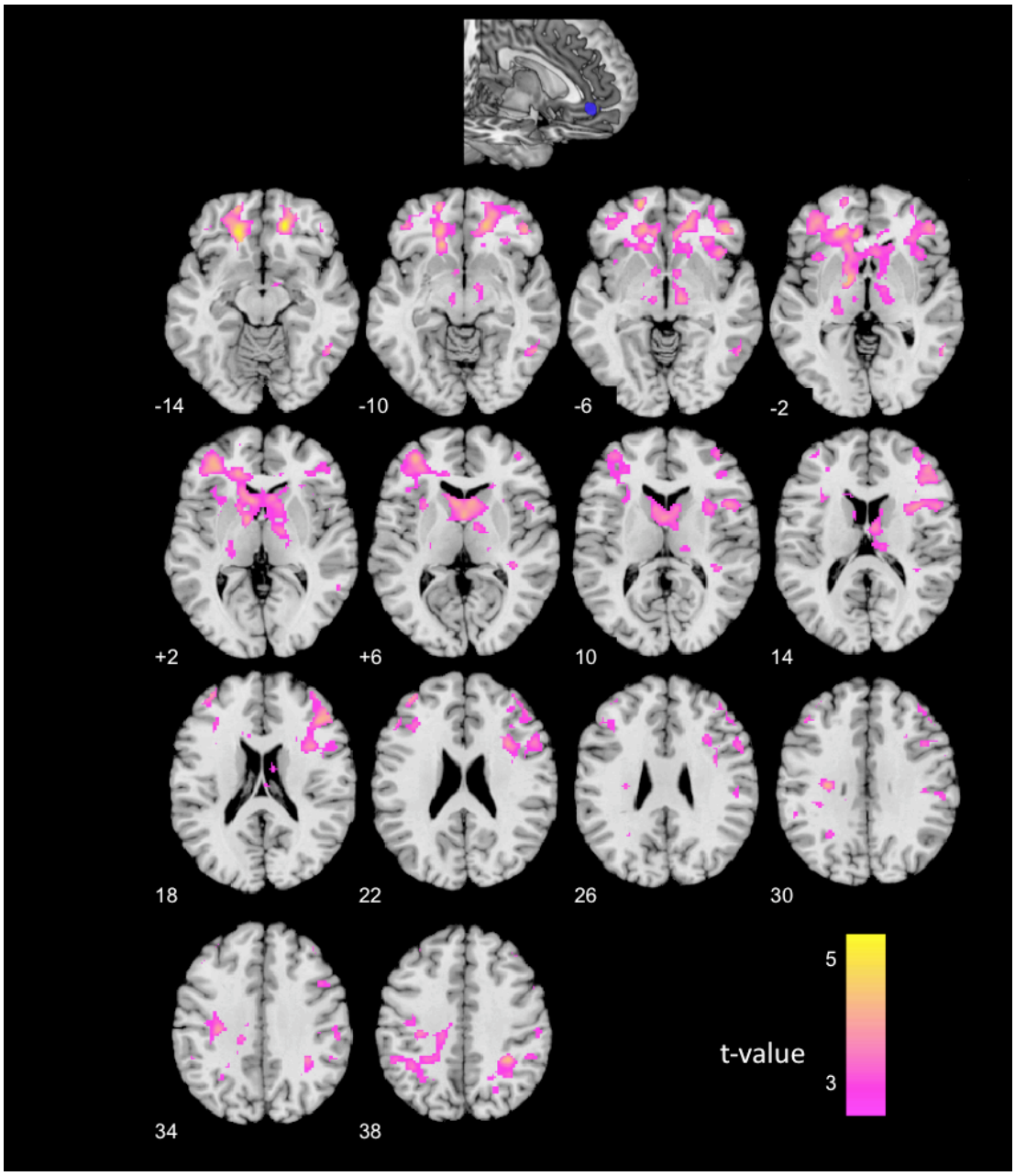

Figure S5. Whole-brain parametric map from a random-effects analysis profiling areas showing increased functional connectivity with a perigenual anterior cingulate cortex (pACC) seed (shown at top). For illustrative purposes, this whole-brain connectivity map is displayed at an uncorrected threshold of $P<0.005$ and a cluster extent of $k > 50$ voxels. Table S4(a) provides Brodmann areas, MNI coordinates, and *t*-values for voxels of peak connectivity (global maxima) profiled. Values beneath each slice correspond to *z* coordinates in MNI space.

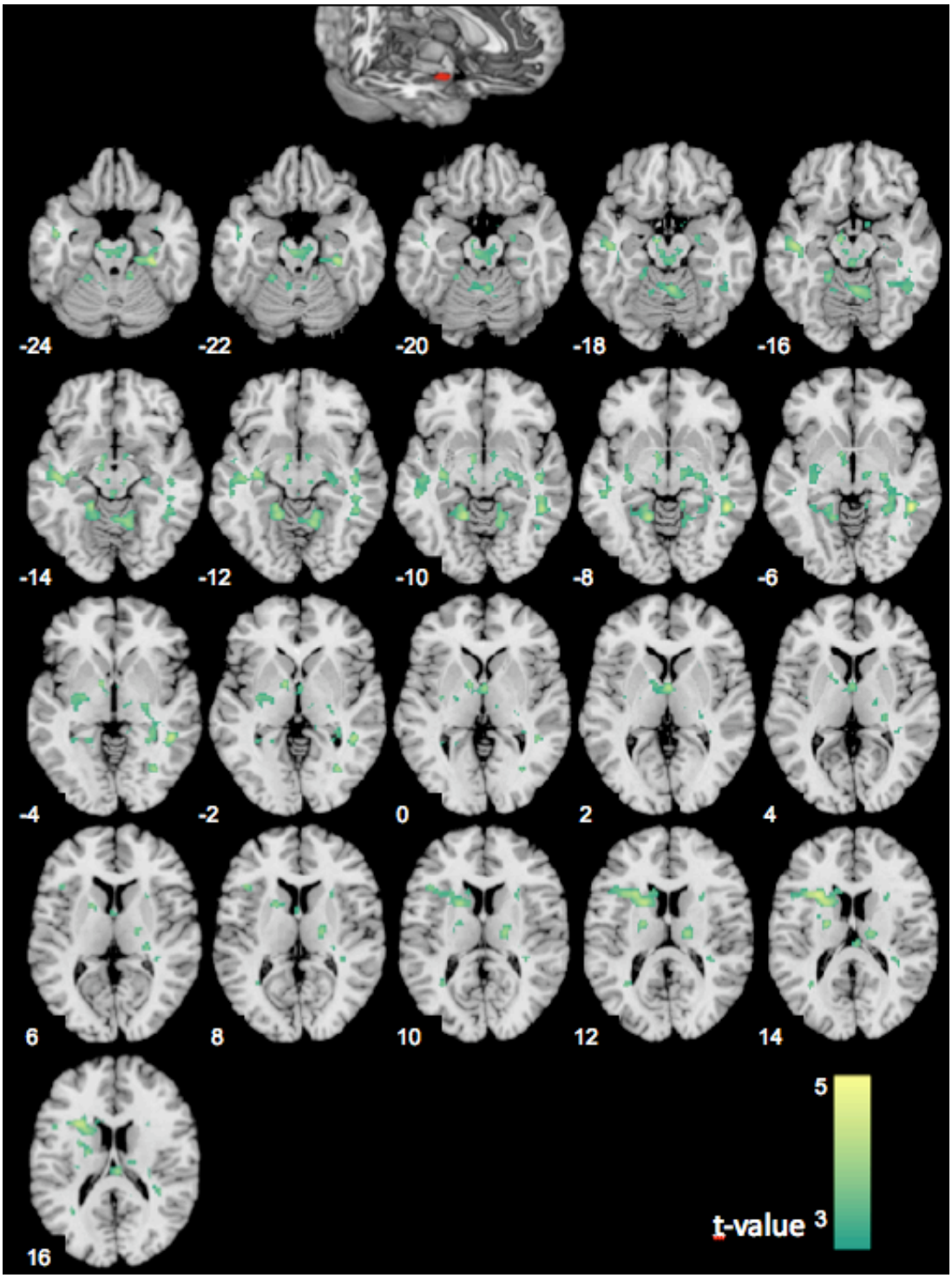

Figure S6. Whole-brain parametric map from a random-effects analysis profiling areas showing increased functional connectivity with an amygdala seed (shown at top). As in Figure S5, the map is displayed at an uncorrected threshold of $P<0.005$, with a combined cluster extent threshold of $k > 50$ voxels. Table S4(b) provides Brodmann areas, MNI coordinates, and *t*-values for voxels of peak connectivity (global maxima) profiled. Values beneath each slice correspond to *z* coordinates in MNI space.

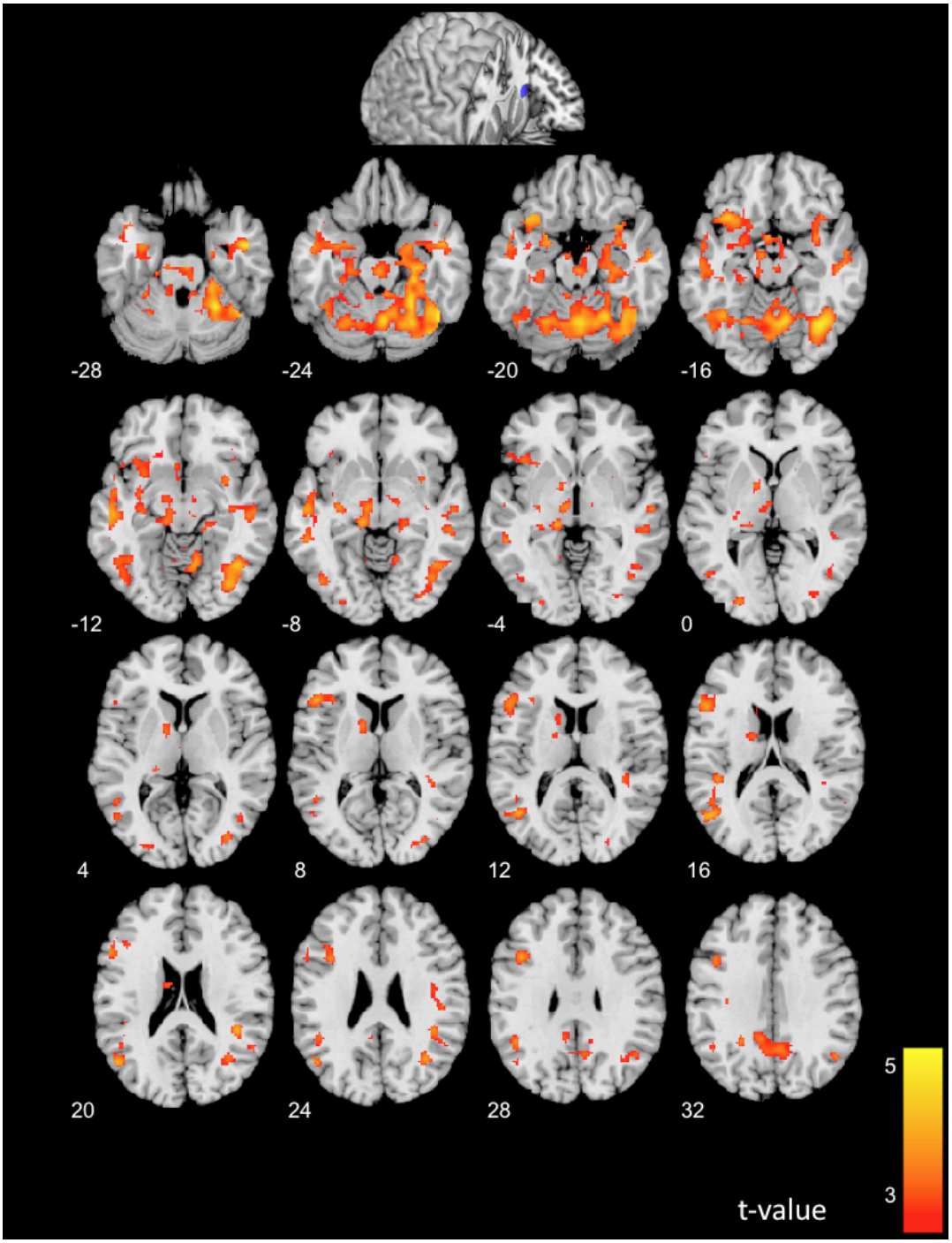

Figure S7. Whole-brain parametric map from a random-effects analysis profiling areas showing increased functional connectivity with a left anterior insula seed (shown at top). As in other supplemental figures for connectivity analyses, the map is displayed at a uncorrected threshold of $P<0.005$, with a combined cluster extent threshold of $k > 50$ voxels. Table S4(c) provides Brodmann areas, MNI coordinates, and *t*-values for voxels of peak connectivity (global maxima) profiled. Values beneath each slice correspond to *z* coordinates in MNI space.

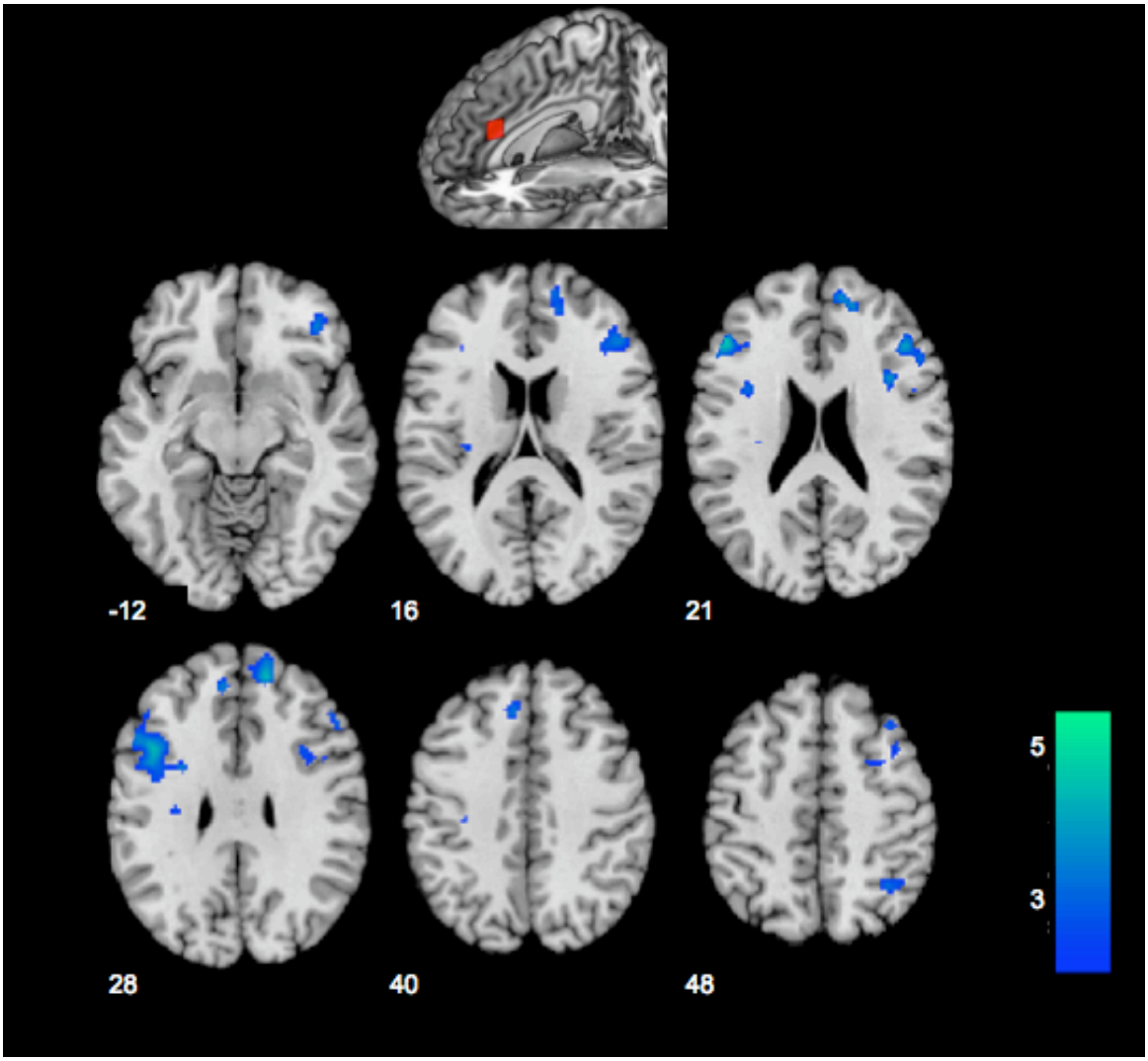

Figure S8. Whole-brain parametric map from a random-effects analysis profiling areas showing increased functional connectivity with a dorsal anterior cingulate seed (shown at top). As in other supplemental figures for connectivity analyses, the map is displayed at a uncorrected threshold of $P<0.005$, with a combined cluster extent threshold of $k > 50$ voxels. Table S4(d) provides Brodmann areas, MNI coordinates, and *t*-values for voxels of peak connectivity (global maxima) profiled. Values beneath each slice correspond to *z* coordinates in MNI space.